Theor Chem Acc (2012) 131:1186
DOI 10.1007/s00214-012-1186-y

REGULAR ARTICLE

Copper coordination to the putative cell binding site of angiogenin: a DFT investigation

Luca Bertini · Maurizio Bruschi · Marco Romaniello · Giuseppe Zampella · Matteo Tiberti · Valentina Barbieri · Claudio Greco · Diego La Mendola · Raffaele P. Bonomo · Piercarlo Fantucci · Luca De Gioia

Received: 29 July 2011 / Accepted: 7 December 2011 / Published online: 3 March 2012

Abstract We present a DFT study of the structural and spectroscopic properties of the complex formed by Cu^{2+} with the peptide fragment Ac-PHREN-NH_2, which encompasses the putative cell binding domain of angiogenin, as well as with its Ac-PHRQN-NH_2 variant. Analysis of structures, energies and spectroscopic parameters has allowed to conclude that the metal coordination environment at pH 8 is formed by a nitrogen atom of His, two deprotonated amide groups, and an oxygen atom from the COO^- side chain of Glu, in nice agreement with recent experimental results (La Mendola et al. in Dalton Trans, 39:10678, 2010). Moreover, DFT results allowed to reveal that the Glu side chain of the Ac-PHREN-NH_2 peptide is coordinated in equatorial position, in a tetrahedrically distorted square planar arrangement, fully disclosing the effects of Cu^{2+} binding on the structural properties of this key angiogenin portion. In the Ac-PHRQN-NH_2 variant, the carboxylate group is replaced by a H_2O molecule in a coordination arrangement similar to that of the wild-type system.

Keywords DFT · Bioinorganic chemistry · Copper · Angiogenin

Dedicated to Professor Vincenzo Barone and published as part of the special collection of articles celebrating his 60th birthday.

L. Bertini · M. Romaniello · G. Zampella · M. Tiberti · V. Barbieri · C. Greco · P. Fantucci · L. De Gioia (✉)
Dipartimento di Biotecnologie e Bioscienze,
Università degli Studi di Milano Bicocca,
Piazza della Scienza, 2, 20126 Milan, Italy
e-mail: luca.degioia@unimib.it

M. Bruschi
Dipartimento di Scienze Ambientali, Università degli Studi di Milano Bicocca, Piazza della Scienza, 1, 20126 Milan, Italy

D. La Mendola
Istituto di Biostrutture e Bioimmagini,
CNR, Viale A. Doria 6, 95125 Catania, Italy

R. P. Bonomo
Dipartimento di Scienze Chimiche,
Università degli Studi di Catania, Viale A. Doria 6,
95125 Catania, Italy

1 Introduction

Angiogenesis is a set of functional processes responsible for the formation of new blood vessels from existing ones and is also a key component of the homeostatic process that regulates the distribution of oxygen to tissues [1]. Angiogenesis occurs in several tightly regulated stages that orchestrate a network of cooperative interactions and can be divided in several phases: (1) an initiation phase, characterized by increased vasopermeability; (2) a progression phase, in which proteolytic enzymes that degrade the extracellular matrix and promote endothelial cell migration are produced; (3) a final phase, in which differentiation into new vessels takes place. The latter phase is mediated by molecules that recruit mesenchymal cells to vessel walls [2].

Angiogenin (Ang) is a protein that undergoes nuclear translocation in endothelial cells, where it accumulates in the nucleolus and stimulates rRNA transcription, a rate limiting step in ribosome biogenesis, protein translation, and cell growth [3]. Ang was originally isolated from the conditioned medium of HT-29 human colon adenocarcinoma cells [4]. The mature Ang is a basic, single-chain protein containing 123 amino acids with a molecular weight of about 14.400 Da, and it is a homologue of bovine

pancreatic ribonuclease A. Indeed, its ribonucleolytic activity is rather low, but Ang is essential for angiogenesis and other functions [5]. In fact, Ang belongs to the ribonuclease superfamily, showing 33% sequence identity to the pancreatic ribonuclease A. However, although the crystal structures of human Ang and pancreatic ribonuclease A are highly similar, a notable difference is evident in the ribonucleolytic active site: the pyrimidine binding site of Ang is "obstructed" by the Gln117 residue, explaining its very weak ribonucleolytic activity (about 10^5–10^6 lower than that of RNase A).

Besides its ribonucleolytic activity, binding of Ang to the endothelial cells surface is needed for its biological functions, and amino acid residues from 60 to 68 are critical in this process. Notably, affinity of Ang for endothelial cells is largely increased in the presence of copper ions [6]. In fact, copper has been recognized to be an angiogenic factor, but the mechanism whereby it exerts this function is still not well understood [7, 8]. In particular, Ang binds 2.4 mol of copper per mol of protein, and the metal ion is important for Ang binding to calf pulmonary artery endothelial cells, which increases by 4.3-fold in the presence of Cu^{2+}.

A putative endothelial cell binding domain of Ang is located in a loop exposed to the solvent and largely unstructured in the native protein [9]. The related amino acid sequence (hAng60–68 = KNGNPHREN) contains the prolyl-histidyl (PH) dyad, which is reminiscent of that present in other copper binding proteins, such as prion proteins [10] and the Wilson's and Menkes' ATPases [11]. In this respect, the comparison between Ang and RNase A structures already suggested possible copper binding sites [12]. In fact, RNase A binds copper at several sites including His-12, His-105 and His-119 at pH 5 [13], but Ang features three additional histidine residues that are not present in RNase A: His-8, His-65 and His-84 [14, 15]. The similarity between the copper binding plasma tripeptide Gly–His–Lys and the copper binding site of albumin and α-fetoprotein, where copper binds to a histidyl residue adjacent to a basic residue (Arg or Lys), suggests that His-65, which is adjacent to Arg-66 in Ang, might be involved in copper binding.

Very recently La Mendola et al. [16] reported the synthesis and characterization of the complex formed by the peptide fragments encompassing the sequence hAng64–68 (Ac-PHREN-NH_2; Scheme 1) and the whole sequence hAng60–68 (Ac-KNGNPHREN-NH_2) with copper.

In particular, combined potentiometric and spectroscopic investigations allowed to reveal the species distribution and the coordination environments of the Cu(II) complexes. It turned out that both peptides coordinate Cu^{2+} in a similar fashion. Moreover, thermodynamic and spectroscopic data indicated that the side chains of Glu and

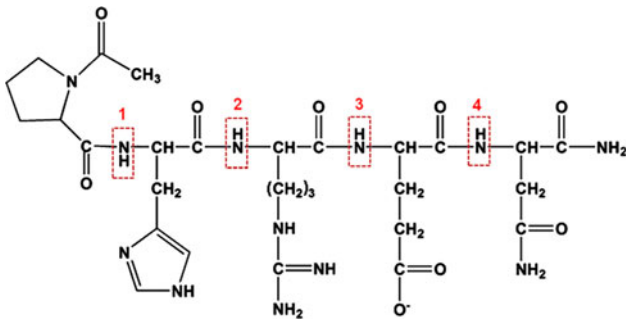

Scheme 1 Structure of the Ac-PHREN-NH_2 peptide. The four NH group of the peptide bonds have been highlighted in *red boxes*

His residues are involved in copper binding at physiological pH. The Cu(II) interaction with the peptide fragment Ang64–68(E67Q) (Ac-PHRQN-NH_2), in which glutamate was substituted by a glutamine residue, was also studied in order to unveil the role of glutamate carboxylate group on Cu(II) coordination. The comparison between results obtained studying the Cu(II) complexes formed by Ac-PHREN-NH_2 and its E67Q variant provided further evidence of the presence of a carboxylate oxygen atom in the copper coordination sphere. On the ground of such results, it was concluded that at pH 8 the metal coordination environment in the complex of Cu(II) with Ac-PHREN-NH_2 is formed by a nitrogen atom of His, two deprotonated amide groups, a water molecule and an oxygen atom from the COO^- side chain of Glu. However, it was not possible to reveal whether the carboxylate oxygen atom was coordinated in equatorial or apical position, hindering the full disclosure of the effects of Cu(II) binding on the structural properties of the Ang60–68 protein portion.

With the aim of complementing available experimental data in the elucidation of the nature of the copper first coordination environment, as well as the apical/equatorial disposition of oxygen ligands, we have carried out a DFT investigation of the Cu(II) complexes formed by Ac-PHREN-NH_2, as well as by the single point mutated peptide Ac-PHRQN-NH_2.

2 Computational details

The generation of the starting structures for DFT optimization was carried out using a combined MM/MD approach. In particular, starting structures, differing for coordination geometry and/or orientation of aminoacid side chains, were initially optimized using the MMFF94x forcefield [17, 18] as implemented in the MOE suite (MOE Molecular Operating Environment, version 2008.10; Chemical Computing Group Inc.: Montreal, Canada, 2008). Then, short 1,000 ps molecular dynamic

simulations were performed at 100 K to relax the systems and allow it to escape from metastable high-energy minima. Simulation temperature was kept very low because the aim of such MM/MD simulations was local (and not global) sampling of the potential energy hypersurface.

Quantum chemical geometry optimizations were carried out using the pure Generalized Gradient Approximation (GGA) BP86 DFT functional [19, 20] and the Resolution of Identity (RI) technique [21], as implemented in the TURBOMOLE suite of programs [22]. Basis sets of triple-zeta plus polarization split valence quality (TZVP hereafter) [23] were adopted for all atoms in the complexes. The DFT grid-size was set to standard m3 value.

The computation of the EPR g tensors and hyperfine coupling constants (hcc) for the ^{63}Cu nucleus has been performed using the B3LYP hybrid functional on the geometries optimized at the RI-BP86/TZVP level. In fact, as shown in a previous DFT investigation about copper coordination to prion protein peptides [24], the structural features (bond distances and angles) of Cu–peptide complexes obtained with B3LYP and BP86 are almost identical. However, BP86 calculations are faster, due to the possibility of using the RI technique, and therefore more suited to test a large number of species, such as in the present work. On the other hand, EPR g tensors and hyperfine coupling constants obtained with B3LYP are in better agreement with experimental data, when compared to BP86 results. An extended basis set (14s, 10p, 5d) [25], augmented by a set of diffuse s, p and d functions (with exponents equal to 0.01, 0.03087, and 0.1, respectively) and contracted to (9s, 7p, 4d), was adopted for the Cu atom. The IGLO-II basis was adopted for all other atoms [26]. EPR hyperfine coupling constants (hcc) were calculated, explicitly taking Spin–Orbit (SO) contributions into account, with the one-centre and mean field approximation (AMFI) [27] for the two electron terms (see Ref. [28] for a complete discussion of the SO operators). For the calculations of g tensors, the gauge origin has been set to the centre of electronic charge. Calculations of EPR properties have been carried out using the ORCA suite of programs [29].

3 Results and discussion

3.1 Geometries and relative energies of isomers of [Cu(Ac-PHREN-NH_2)(H_2O)] and [Cu(Ac-PHRQN-NH_2)(H_2O)]$^{+1}$ complexes

According to the experimental evidences, Cu(II) coordination to the Ac-PHREN-NH_2 peptide at pH 8 involves two N^- anions from the deprotonated amide groups of the peptide bonds, the carboxylate group of Glu and a nitrogen atom from the His side chain. In addition, a water molecule should also be coordinated to the metal ion [16]. Before discussing which deprotonated N^- groups are actually involved in Cu(II) coordination, some considerations are in order. Previous results obtained studying coordination compounds formed by Cu(II) with fragments of the prion protein [24, 30–33], as well as simple considerations about the preferential formation of 5- and 6-member rings when dealing with chelate ligands, lead to the conclusion that the two N^- anions involved in Cu(II) coordination must be contiguous. Therefore, only three configurations are possible, namely those involving the **1–2**, **2–3** or **3–4** deprotonated amide groups (see Scheme 1 for amide groups labeling). We preliminary analyzed the conformation of these three configurations at Molecular Mechanics (MM) level, in order to quickly understand which is the most likely Cu^{2+} coordination geometry. The preliminary MM analysis revealed that, when the **1–2** or **3–4** configurations are taken into account, the histidine (in the **1–2** configuration) or the glutamic acid (in the **3–4** configuration) side chains occupy the apical position in the metal coordination sphere. In fact, since the side chains of His (in the **1–2** configuration) or Glu (in the **3–4** configuration) are in between the deprotonated N^- groups that form the planar 5-member cycle (Scheme 2), the aminoacid side chain must necessarily coordinate Cu^{2+} in apical position due to steric restrictions. As a consequence, in complexes characterized by **1–2** or **3–4** binding mode, the water molecule must occupy an equatorial position in the Cu(II) coordination environment.

MM results also indicate that the **1–2** and **3–4** binding modes induce some strain in the peptide chain. In particular, the side chain of the coordinating aminoacid which does not belong to the five-member ring (Glu in **1–2** complexes, His in **3–4** structures) is far from the metal center and its coordination to the metal atom is always accompanied by some strain of the peptide backbone. MM analysis of the **2–3** binding mode reveals that the imidazole ring of His and the carboxylate group of Glu can occupy equatorial positions in the Cu(II) coordination sphere without inducing steric strain in the molecule. These results suggest that the structures featuring the **2–3** binding mode

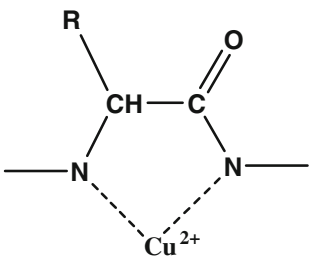

Scheme 2 Five-member ring formed in Ac-PHREN-NH_2 upon coordination to Cu(II) of the two adjacent deprotonated amide groups

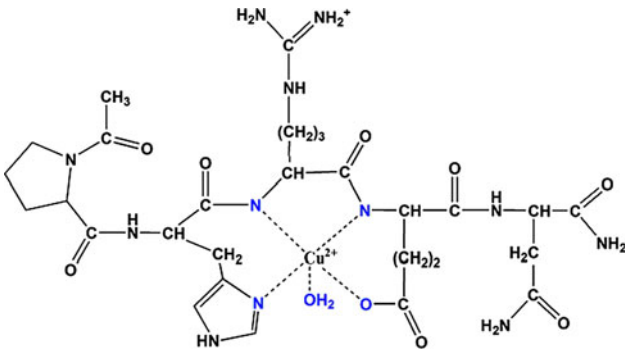

Scheme 3 Schematic representation of the **2–3** binding mode in complexes between Cu(II), the peptide Ac-PHREN-NH_2 and a water molecule

most likely correspond to the lowest-energy isomers (see Scheme 3).

Therefore, we have carried out a thorough DFT investigation into the conformational properties of coordination compounds featuring the **2–3** binding mode. However, for the sake of completeness, we have evaluated by DFT also some structures characterized by the **1–2** or **3–4** binding mode, to quantify the strain of the peptide chain.

To select reasonable starting structures for DFT optimization, we have carried out classical MD simulations (see "Computational details") of the [Cu(Ac-PHREN-NH_2)(H_2O)] complex featuring the **2–3** binding mode, selecting snapshots along the MD trajectory which correspond to low-energy conformations. The protocol adopted to explore the configurational space of the system is the following. The structures characterized by the **2–3** binding mode can be ideally divided into two families: the first containing structures featuring an apical water molecule (and consequently an equatorial Glu side chain), and the second containing structures featuring an equatorial water molecule (Scheme 4).

We initially generated "ideal" (dihedral angle of the base of the pyramid equal to zero, molecular axes of the apical ligand exactly perpendicular to the base) structures characterized by the N_3O_2 coordination environment and

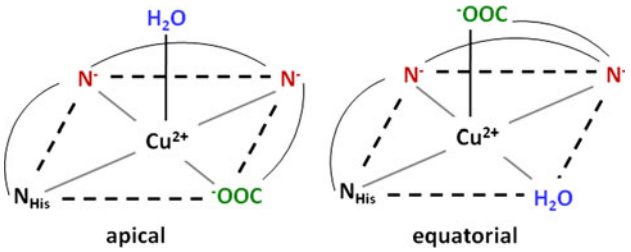

Scheme 4 The two families of [Cu(Ac-PHREN-NH_2)(H_2O)] complexes characterized by the **2–3** binding mode. Apical and equatorial labels are referred to the position of the water molecule in the Cu^{2+} coordination sphere

featuring an apical or equatorial water molecule. The value of Cu–N^- distances has been set to 2.000 Å, according to the BP86 optimized Cu–N distances in the [Cu(HGGG)] system [33]. For the Cu–N_{His} and Cu-O^-_{Glu} distances, we adopted the value of 1.894 and 2.007 Å obtained, respectively, from BP86/TZVP gas-phase optimization of the Cu-His and Cu-Glu adducts. Regarding the Cu-O distance to describe Cu–H_2O binding, we considered as experimental reference the XRD value of 2.4 Å in *cis*-Cu(Gly)$_2$·H_2O, which fits well also with the analysis of Sobolović et al. [34], which measured a mean value of 2.4 ± 0.1 Å for Cu-O distances in 10 aminoacid/water Cu(II) complexes.

Using the two "ideal" structures as templates, we generated apical and equatorial conformations from molecular dynamics simulations in which the Cu(II) coordination distances were constrained to the above-mentioned reference values. Then, for each structure obtained, we first optimized its geometry at the MM level of theory, and the corresponding minimum energy structure was used as starting point of a two-step DFT optimization. In the first step, the Cu(II) coordination was constrained, allowing only the peptide moiety to relax. In the second step, the whole geometry was optimized removing the constraints.

The relevant optimized geometry parameters, as well as computed relative energies of all structures characterized by the **2–3** binding mode are collected in Table 1. It must be noted that in structures characterized by an apical water molecule, the N_3O_2 coordination can be realized only in one way, whereas in the case of equatorial water binding, the isomer shown in Scheme 4 is not the only plausible possibility, but other three ligands arrangements, referred to as the A, B and C, can in principle exist (Scheme 5).

Before discussing the fine details of the various structures optimized, it is interesting to highlight some trends obtained by our DFT investigation. Except for a few structures, geometry optimizations usually led to tetrahedral distortion of the initial square pyramidal coordination. In addition, the H_2O ligand often resulted loosely bound or non-bound to Cu(II), yielding 4-coordinated N_3O structures. It is also worth noting that when starting from structures featuring an equatorial water ligand, the H_2O molecule always left the Cu(II) coordination sphere, and it was replaced in the equatorial position by the oxygen atom of the glutamic acid residue. Therefore, structures characterized by equatorial coordination of the H_2O molecule should not correspond to stable forms of the [Cu(Ac-PHREN-NH_2)(H_2O)] complex.

In the exploration of the conformation space of [Cu(Ac-PHREN-NH_2)(H_2O)], we often found that structures differ only for the number of intramolecular H-bonds. As shown in the following, when a complex is explicitly solvated by a reasonable number of H_2O molecules, intramolecular interactions are often lost because the side chains of the

Table 1 Selected geometrical parameters (in Å and degree) and energy differences relative to the lowest-energy form (in kcal mol^{-1}) of the [Cu(Ac-PHREN-NH_2)(H_2O)] isomers

Isomer	Distances								
	CN	ΔE	Cu−O_{H_2O}	Cu-O_{CO}	Cu–N_1^-	Cu–N_2^-	Cu–N_{His}	δ Dihedral	H-bonds
2–3 Binding mode									
1	5	0.0	2.645	2.039	2.016	2.019	2.039	0.4	6
2	4	2.0	3.777	2.001	2.017	2.001	2.000	16.6	5
3	4	2.1	3.863	2.012	2.020	2.000	2.006	12.4	5
4	4	2.1	3.796	2.010	2.012	1.999	1.994	13.5	5
5	4	5.5	3.565	2.001	1.996	1.948	2.016	38.5	2
6	4	6.0	3.374	1.973	1.965	2.034	2.003	9.2	4
7	4	6.2	3.354	1.999	2.029	2.033	2.032	17.6	4
8	5	6.3	2.488	2.014	2.017	2.056	2.029	0.9	3
9	4	8.4	3.684	1.983	1.986	2.022	2.012	8.7	4
10	4	12.2	3.655	1.982	1.932	2.074	1.986	42.1	8
11	5	12.7	2.492	2.020	1.994	2.070	2.028	4.3	5
12	5	13.7	2.348	2.044	2.037	2.023	1.971	3.4	4
13	4	14.0	3.390	2.002	1.963	1.929	2.100	37.3	3
14	5	14.8	2.753	2.009	2.032	1.993	2.047	1.3	6
15	4	15.3	3.912	1.954	1.954	2.016	2.021	35.3	5
16	4	15.5	3.755	2.010	1.990	2.019	2.011	18.2	5
17	4	16.0	3.924	1.962	1.949	2.023	2.020	34.9	5
18	4	17.7	4.073	1.932	1.972	2.002	2.038	35.2	6
19	5	24.6	2.889	1.997	2.000	2.013	2.054	19.6	4
20	5	32.3	2.407	1.997	2.000	2.004	1.994	0.4	6
2–3 Binding mode									
21	5	13.7	2.031	2.042	1.984	2.150	2.281	11.0	8
22	5	13.8	2.023	2.042	1.982	2.130	2.326	14.4	8
23	5	20.0	2.020	2.050	2.050	2.004	2.302	9.6	4
24	4	22.3	1.994	2.041	1.977	1.976		44.0	5
25	4	25.4	1.979	2.070	1.987	1.968		47.2	6
26	5	26.7	2.014	2.112	2.029	2.038	2.237	38.9	6
27	4	26.8	1.973	1.998	1.998	1.985		30.6	3
28	5	31.2	2.017	1.989	2.107	2.063	2.084	47.5	4
3–4 Binding mode									
29	5	8.1	2.450	2.242*	1.931	1.999	2.050	31.0	5
30	3	9.7	3.075		1.915	2.023	1.978		6
31	5	16.4	2.544	2.178*	2.012	1.927	2.024	19.7	5
32	5	26.1	2.170	2.010	2.000	2.078	2.168	47.5	5
33	5	26.2	3.414	2.574 2.711*	1.935	1.986	2.003	53.7	6
34	5	35.2	3.641	2.085 1.996*	1.911	1.993		28.8	5
35	5	36.1	2.035	2.054	1.999	2.073	2.294	14.3	5
36	5	37.3	2.289	2.627*	2.071	1.923	2.018	16.3	5
37	5	38.1	2.142	2.088	2.003	2.054	2.227**	21.0	5
38	5	39.4	2.041	2.142	1.984	2.058	2.287	55.6	4
39	5	41.6	5.610	1.995	1.969	2.038	2.033	36.9	6
40	5	42.4	2.289	2.267*	2.020	1.940	2.035	16.3	3
41	5	50.6	2.165	2.306	2.000	2.023	2.025	20.6	3
42	5	51.2	3.889	1.993	1.983	2.053	2.222	58.3	3

In the table are reported the five Cu-L distances, the dihedral angle that defines the base of the square pyramid of the N_3O_2 coordination sphere and the number of hydrogen bonds (H···O distance less than 2.0 Å). *CN* stands for coordination number

* The oxygen atom coordinated to Cu^{2+} does not belong to the COO^- group of the Glu side chain residue

** Histidine in apical position

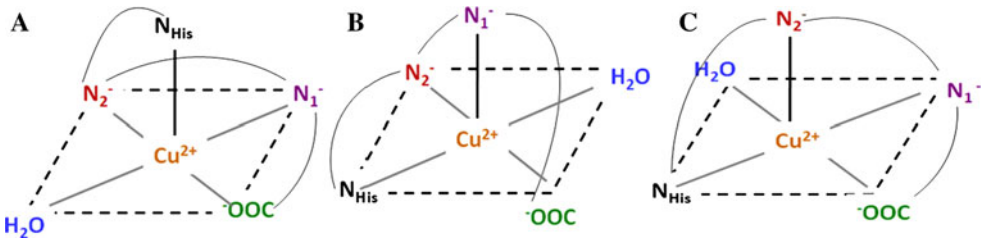

Scheme 5 The three subfamilies of [Cu(Ac-PHREN-NH_2)(H_2O)] complexes characterized by the **2–3** binding mode and the water molecule in equatorial position

residues not involved in Cu(II) coordination (in particular arginine) prefer to form H-bonds with the solvent. Nevertheless, even if we are aware of the limits of such approach, we carried out most DFT calculations neglecting solvent effects. In fact, the explicit description of a shell of water molecules surrounding the [Cu(Ac-PHREN-NH_2)(H_2O)] complex would be computationally too demanding. Indeed, since one of the main purposes of this study was the elucidation of the position of the H_2O ligand in the Cu(II) coordination sphere, in principle, solvent effects due to bulk water could be described using an implicit solvent model. However, it was already observed that DFT tends to underestimate H_2O–Cu(II) binding in similar complexes [33], and we noted that the adoption of an implicit solvent model makes the H_2O–Cu(II) bond even weaker (vide infra), not allowing to properly study H_2O coordination to Cu(II) in this class of compounds.

The lowest-energy structure characterized by the **2–3** binding mode features an apical water molecule (**1**; Fig. 1). In **1**, the N_3O_2 square pyramidal Cu(II) coordination environment is characterized by a dihedral angle δ (defined by the atoms N_{HIS}–N_1^-–N_2^-–O^- forming the base of the square pyramid) equal to 0.4°, and a Cu−O_{H_2O} distance = 2.645 Å. Other five structures are characterized by a Cu−O_{H_2O} distance lower than 3.0 Å (**8**, **11**, **12**, **14**, **19**; Table 1). When compared to **1**, these structures are characterized by a smaller number of H-bonds, except for structure **14**, which, however, is characterized by a loosely bound H_2O molecule (Cu−O_{H_2O} = 2.753 Å). The structure with the shortest Cu−O_{H_2O} distance (**12**) features an apical water molecule and is 13.7 kcal mol^{-1} higher in energy than **1**. In this context, it is also worth noting that **1** and **12** differ for the number of intramolecular H-bonds (4 in **12**, 6 in **1**; d(H···O) ≤ 2.0 Å), underlying the role played by this type of interactions for the relative energies of the structures considered.

The electronic spectra of Ac-PHREN-NH_2 and the lowest-energy [Cu(Ac-PHREN-NH_2)(H_2O)] form (structure **1**) have been computed at BP86/TZVP TDDFT level and are shown in Fig. 2. The first 100 transitions have been

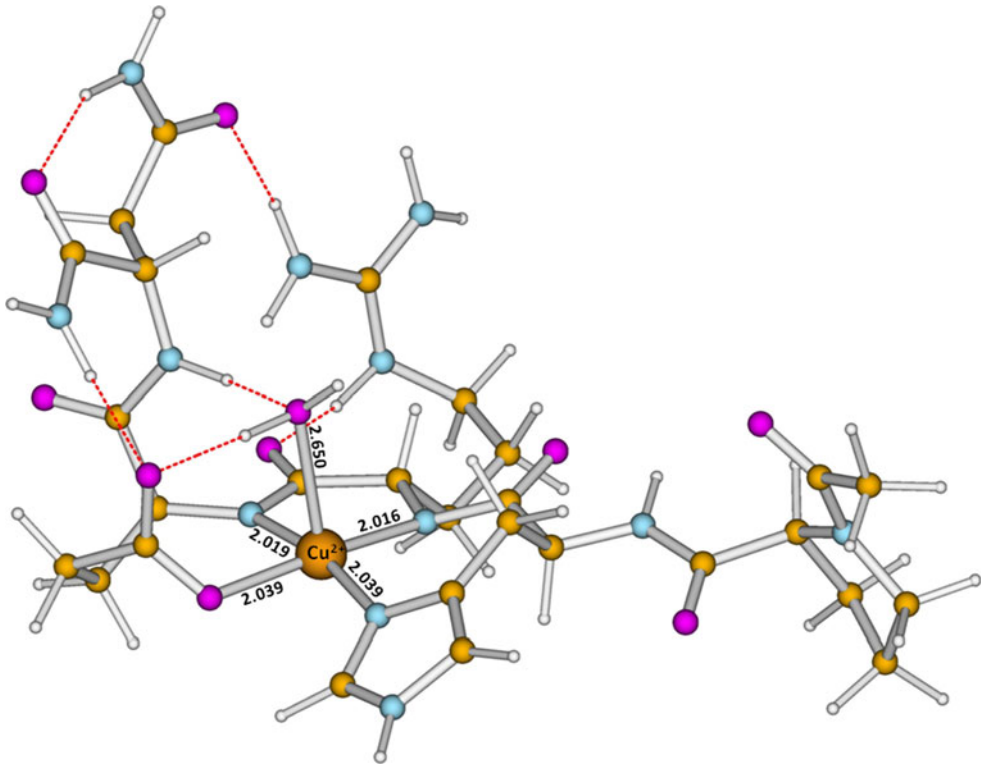

Fig. 1 Lowest-energy structure of the [Cu(Ac-PHREN-NH_2)(H_2O)] complex characterized by the **2–3** binding mode (**1**). Distances in Å

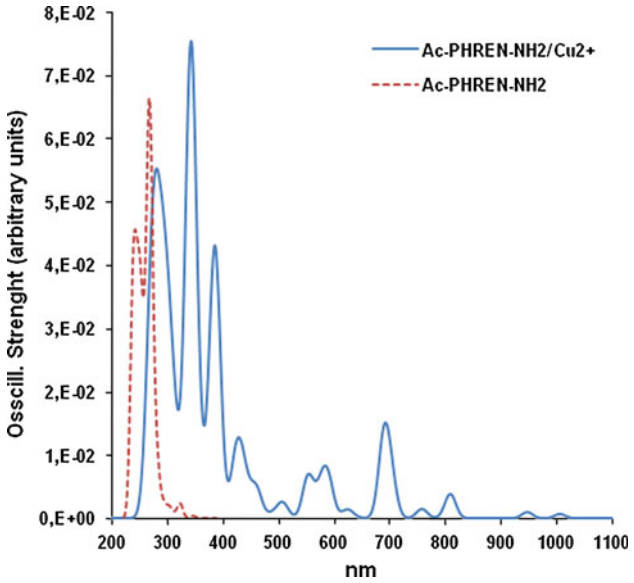

Fig. 2 TDDFT computed UV–Vis spectra for Ac-PHREN-NH_2 and the lowest-energy structure of the [Cu(Ac-PHREN-NH_2)(H_2O)] complex (**1**)

computed, and excitation energies, corresponding oscillation strengths and MO compositions for the first 30 transitions are collected in Table 2. It must be noted that the BP86 functional is not the optimal choice to reproduce excitation energies, in particular when metal-to-ligand charge transfer (MLCT) bands are considered, but the large size of the systems investigated did not allow us to adopt more suited functional, as PBE0 [35]. In any case, it can be concluded that computed UV–Vis bands of Ac-PHREN-NH_2 are mainly due to the histidine residue and correspond to two intense absorptions at 266 and 240 nm, and one weak band at 320 nm. In the corresponding Cu(II) complex, the two intense bands are red-shifted by about 100 nm. The bands in the range 1,000–500 nm (Table 2) are of SOMO-n(β) → SUMO(β) type ($n = 0$–14, Singly Occupied and Singly Unoccupied MO, respectively) and essentially correspond to the Cu(II) d–d transitions. In particular, the first five transitions that involve the d-Cu(II) MOs are of d–d type. The most intense band is at 689 nm (excitation 6), in fairly good agreement with the 640 nm absorption reported by La Mendola et al. [16].

As already pointed out, **2–3** isomers characterized by equatorial disposition of the water molecule do not correspond to minima on the potential energy surface, suggesting an intrinsic instability of this coordination mode. In order to quantify the destabilization of structures featuring an equatorially coordinated water molecule, we have also optimized a structure (**20**), which is obtained from **1** after exchange of the positions of the water molecule and the carboxylate group. In order to maintain the Cu(II) coordination environment, the position of the two coordinated

Table 2 TDDFT BP86/TZVP electronic spectrum of **1**

Transition	nm	f	$a \rightarrow i$
1	1,005	7×10^{-4}	$202\beta \rightarrow 203\beta$
2	947	1×10^{-3}	$201\beta \rightarrow 203\beta$
3	808	4×10^{-3}	$200\beta \rightarrow 203\beta$
4	757	2×10^{-3}	$199\beta \rightarrow 203\beta$
5	702	5×10^{-3}	$198\beta \rightarrow 203\beta$ (55%)
			$198\beta \rightarrow 203\beta$ (45%)
6	689	1×10^{-2}	$197\beta \rightarrow 203\beta$ (45%)
			$198\beta \rightarrow 203\beta$ (33%)
7	685	2×10^{-3}	$196\beta \rightarrow 203\beta$ (83%)
8	637	2×10^{-4}	$195\beta \rightarrow 203\beta$
9	623	1×10^{-3}	$194\beta \rightarrow 203\beta$
10	597	2×10^{-4}	$193\beta \rightarrow 203\beta$
11	588	5×10^{-3}	$192\beta \rightarrow 203\beta$
12	575	4×10^{-3}	$191\beta \rightarrow 203\beta$
13	552	6×10^{-3}	$190\beta \rightarrow 203\beta$
14	507	2×10^{-3}	$189\beta \rightarrow 203\beta$
15	497	5×10^{-4}	$188\beta \rightarrow 203\beta$
16	485	5×10^{-4}	$187\beta \rightarrow 203\beta$
17	462	9×10^{-4}	$185\beta \rightarrow 203\beta$ (62%)
18	457	4×10^{-3}	$186\beta \rightarrow 203\beta$ (87%)

For each transition, the excitation energy (nm), the oscillation strength (f) and the main ($a \rightarrow i$) monoelectronic excitations with the corresponding percentage composition are reported

oxygen atoms from the water molecule and the carboxylate group have been constrained to the Cu-O distances observed in **1**. Although this evaluation is qualitative, we found that structure **20** is more than 30 kcal mol^{-1} higher in energy than **1**.

In order to evaluate whether an extra water molecule might be bound to Cu(II), leading to a pseudo-octahedral coordination environment, we further investigated complex **1** after addition of a second H_2O molecule in apical position. However, the optimization of such a species led to a square pyramidal structure in which the extra water molecule moved away from the metal atom (final $Cu-O_{H_2O}$ distance = 3.567 Å).

Going back to the issue of the computational approach adopted in this study to describe solvation effects, we also optimized the lowest-energy structure (**1**) including solvent effects through the implicit solvent model COSMO (COnductor-like Screening MOdel) [36–38]. The main effect observed in COSMO calculations was the removal of the H_2O molecule from the Cu(II) coordination sphere, which consequently becomes tetrahedrally distorted (δ moves from 0.4 to 30.7°) .

Finally, we have also evaluated the lowest-energy complex **1** when explicitly solvated (**1 W**). To address this point, structure **1** was solvated with a cluster of 55 H_2O

molecules, whose position was optimized by mean of a short MD simulation (1,500 ps) and successive MM geometry optimization. The solvated structure obtained in this way was successively optimized at DFT level using the same level of theory adopted for the non-solvated models (BP86/TZVP). Upon geometry optimization, the Cu(II) coordination does not change significantly. The H_2O molecule initially at 2.645 Å gets closer to the metal center (2.445 Å) and the δ dihedral angle increases of only 2°. Notably, no intramolecular H-bonds are found because the aminoacid side chains are all involved in H-bond with the solvent.

DFT results obtained studying structures characterized by the **1–2** and **3–4** binding mode indicate that these isomers are higher in energy with respect to the lowest-energy **2–3** isomer (**1**). In particular, most of the **1–2** structures (**21**, **22**, **23**, **26** and **28**; Table 1) feature a Cu(II) coordination with the histidine residue in apical position (see Scheme 6) and are higher in energy with respect to isomer **1** by at least 13.7 kcal mol^{-1}.

The three lowest-energy **1–2** structures feature square pyramid coordination with a small tetrahedral distortion. The lowest-energy **1–2** form (structure **21**) is shown in Fig. 3. It is interesting to point out that the H_2O ligand is coordinated to Cu(II) with a much shorter Cu-O distance (2.031 Å) compared with the **2–3** structures. In fact, in **21**, the Cu(II)–H_2O binding is "assisted" by the formation of two H-bonds formed with the two CO groups of the Glu side chain and the peptide bond between Pro and His (Scheme 7).

During the conformational sampling of structures characterized by the **1–2** binding mode, we have found three 4-coordinated structures (**24**, **25** and **27**), in which the histidine side chain is not coordinated to Cu(II). However, these isomers are at least 8.6 kcal mol^{-1} higher in energy than the lowest-energy **1–2** form (**21**).

The analysis of the MD simulations of the **3–4** configuration revealed a larger number of possible copper coordinations. In particular, several structures obtained from the MD simulations can be classified in two families (Scheme 8).

In structures **29**, **31**, **36** and **40** (Scheme 8; family *a*), the carboxylate of the glutamic acid forms an electrostatic interaction with the side chain of arginine, and consequently the carbonyl group of the C-terminal amide group enters the Cu(II) coordination sphere in equatorial position. Among the family *a* species, structure **29** is the lowest in energy (+8.1 kcal mol^{-1} with respect to **1**).

In structures **32**, **35**, **38**, **41** and **43** (Scheme 8; family *b*), the carboxylate group of Glu is coordinated to Cu(II) in apical position, and therefore the water molecule occupies the equatorial position. All these structures are genuine equatorial forms, but, however, are even higher in energy than the constrained **2–3** equatorial form (structure **20**).

The other **3–4** isomers obtained from the conformational sampling are higher in energy and feature a different Cu(II) coordination environment. It is worth noting that the 3-coordinated structure **30** ($2N^-$ and N_{His}) lies only 1.6 kcal mol^{-1} higher in energy with respect to the lowest-energy **3–4** structure (**29**) because it is stabilized by the formation of 6 intramolecular H-bonds. Structures **33** and **34**, which are characterized by the substitution of the coordinated H_2O with a CO group of the peptide chain, lie at least 29.6 kcal mol^{-1} higher in energy with respect to **1**. In **34**, also the histidine side chain leaves the Cu(II) coordination sphere, giving a 4-coordinated form. Structure **37** is the only **3–4** form that features the histidine side chain in apical position, similar to the **1–2** forms.

In order to better understand the role of the glutamate side chain in Cu(II) binding, and prompted by the previous observation that cleavage of the E67–N68 peptide bond compromises the angiogenic activity of Ang [39], La Mendola et al. [16] investigated also Cu(II) binding to the $E \rightarrow Q$ variant of the Ac-PHREN-NH_2 peptide ($[Cu(Ac\text{-}PHRQN\text{-}NH_2)(H_2O)]^{+1}$) observing at pH 8 a value of the $A_{\parallel}$ component of the ^{63}Cu hyperfine coupling constant slightly larger than that measured for the wild-type species.

In principle, four different types of coordination can be observed in complexes between Cu(II) and Ac-PHRQN-NH_2 (Scheme 9), in which the glutamine residue can be coordinate to Cu(II) via the NH_2 or CO group of its side chain, and the H_2O ligand can occupy apical or equatorial position. As well know from experimental evidences at neutral pH, the amidic NH_2 group should not coordinate the Cu(II) ion. However, to test the computational approach employed in this investigation, it is interesting also to consider this type of coordination. Sampling of the configuration space of the $[Cu(Ac\text{-}PHRQN\text{-}NH_2)(H_2O)]^+$ complex has been carried out using the same approach adopted for the wild-type peptide. In particular, starting from the lowest-energy forms of the Ac-PHREN-NH_2 complex, we introduced the E → Q substitution and successively carried out

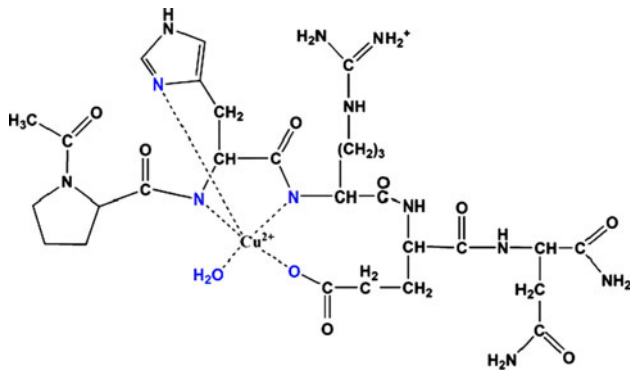

Scheme 6 Schematic representation of the **1–2** binding mode in complexes between Cu(II), the peptide Ac-PHREN-NH_2 and a water molecule

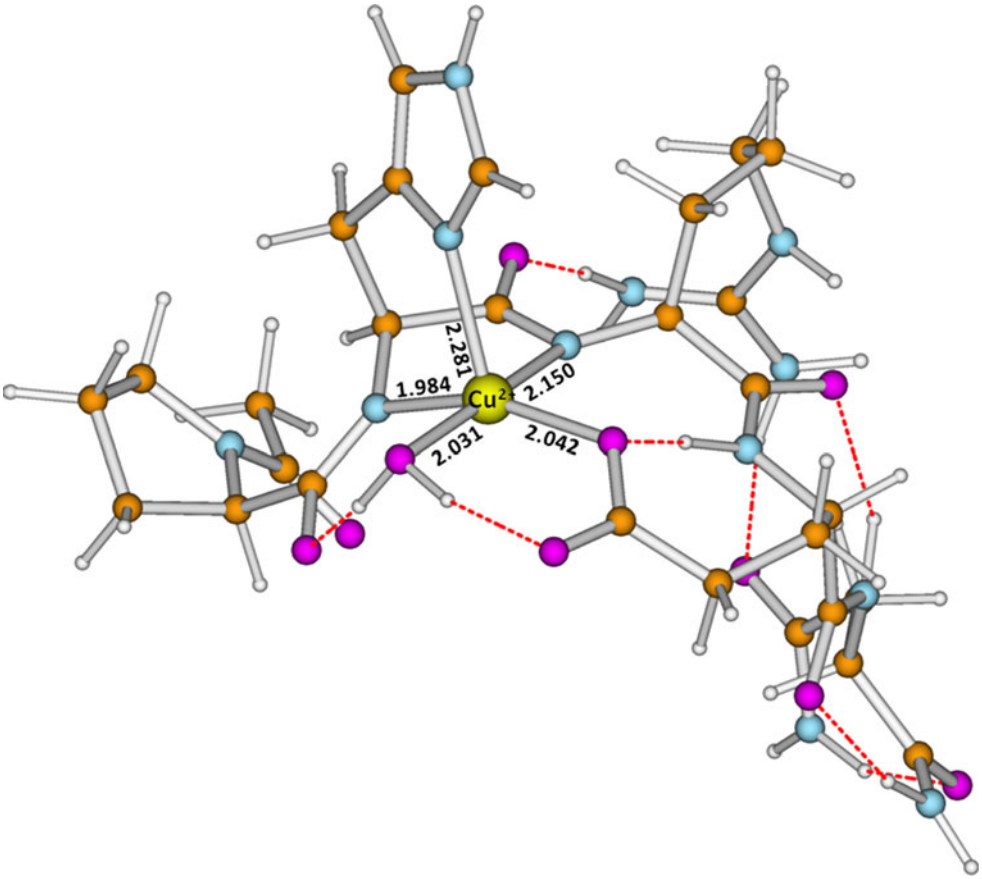

Fig. 3 Lowest-energy structure of the [Cu(Ac-PHREN-NH_2)(H_2O)] complex characterized by the **1–2** binding mode (**21**). Distances in Å

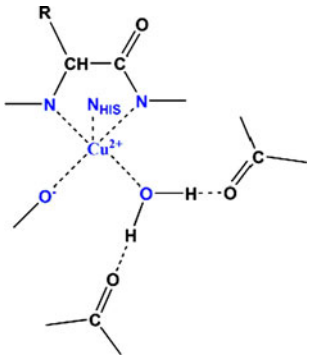

Scheme 7 Schematic representation of the Cu(II) coordination environment in the lowest-energy complex characterized by the **1–2** binding mode (structure **21**)

MD simulations to obtain starting point structures for DFT optimizations. We extracted from the MD trajectories 8 isomers characterized by apical (4 structures) or equatorial (4 structures) H_2O coordination, and for each structure, we evaluated both CO and NH_2 coordination of the glutamine side chain, obtaining a total number of 16 starting point structures for DFT optimization.

In general, in structures characterized by coordination of the NH_2 group of Gln, the Cu–N distance is about 2.3 Å and the NH_2 group is in equatorial position. The corresponding forms in which the CO amidic group is coordinated in equatorial position to Cu^{2+} feature a Cu-O distance within 2.1–2.2 Å.

Scheme 8 Schematic representation of the two families of complexes between Cu(II), the peptide Ac-PHREN-NH_2 and a water molecule, characterized by the **3–4** binding mode

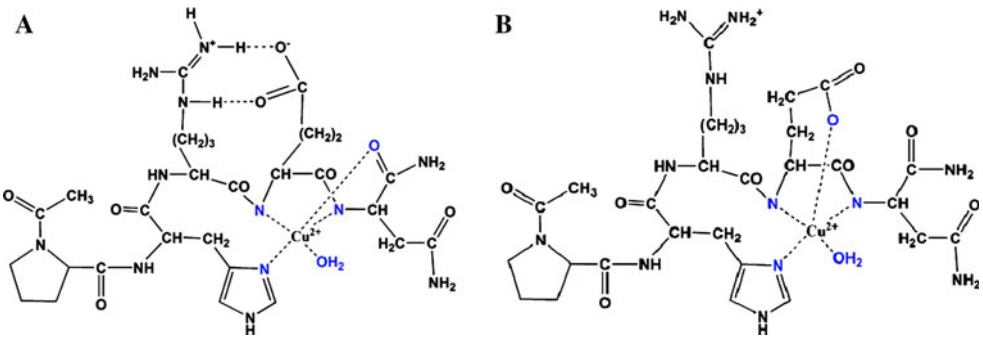

Relative energies of the various DFT optimized structures, as well as relevant bond distances for [Cu(Ac-PHRQN-NH_2)(H_2O)]$^{+1}$ complexes are collected in Table 3. Notably, all [Cu(Ac-PHRQN-NH_2)(H_2O)]$^{+1}$ low-energy structures are characterized by a significant tetrahedral distortion. The lowest-energy [Cu(Ac-PHRQN-

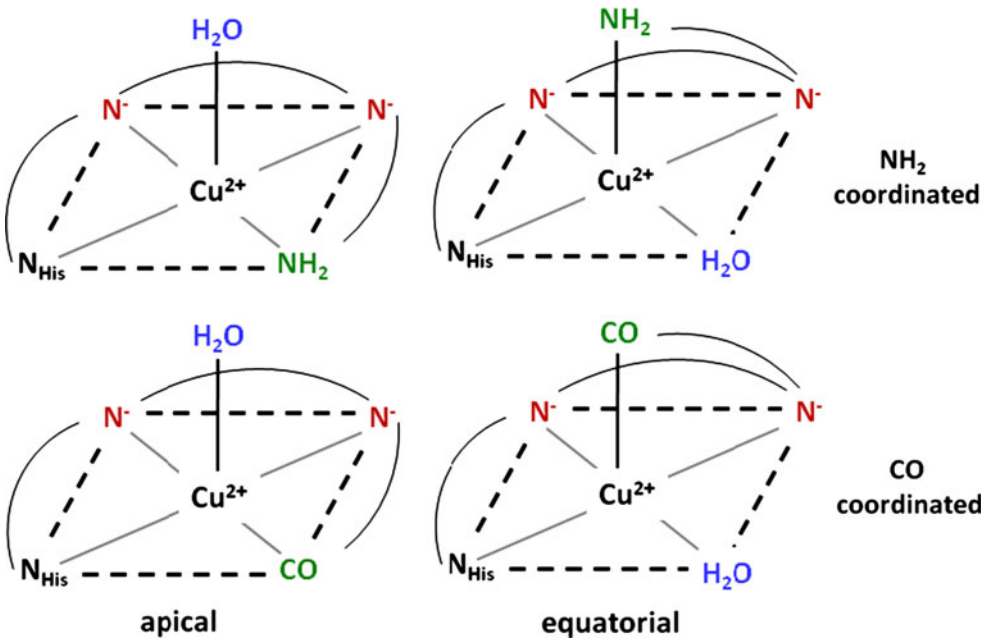

Scheme 9 The four conformation subfamilies of the [Cu(Ac-PHRQN-NH_2)(H_2O)]$^{+1}$ complex. The labels apical and equatorial are referred to the position of the water molecule in the Cu^{2+} coordination sphere

Table 3 Selected geometrical parameters (in Å and degree) and energy differences relative to the lowest-energy form (in kcal mol^{-1}) of the [Cu(Ac-PHRQN-NH_2)(H_2O)]$^{+1}$ complexes

Isomer	Distances								
	CN	ΔE	Cu−O_{H_2O}	Cu-O_{CO}	Cu–N_1^-	Cu–N_2^-	Cu–N_{His}	δ Dihedral	H-bonds
Q1	5	0.0	2.198		2.278	1.969	2.044	2.024	25.2
Q2	5	1.3	2.301		2.341	2.013	1.973	2.001	20.4
Q3	4	2.2	2.124			1.992	2.001	2.027	16.6
Q4	5	7.1	2.257		2.348	2.049	1.954	1.997	29.5
Q5	4	10.3	2.174			1.997	1.947	1.992	40.8
Q6	5	11.0	2.242		2.252	2.022	1.994	2.012	39.4
Q7	4	13.2	3.495		2.201	1.928	1.992	1.976	37.5
Q8	5	15.2	2.484	2.317		2.026	1.970	2.035	21.4
Q9	5	15.2	2.537	2.302		1.966	2.023	2.031	20.7
Q10	4	16.8	4.652		2.134	1.998	1.931	1.968	29.6
Q11	5	17.9	2.738		2.203	2.060	1.932	1.978	16.3
Q12	3	19.2	4.123			1.972	1.915	1.939	
Q13	4	20.1	4.199	2.273		1.955	2.000	1.998	9.0
Q14	4	21.9	3.668	2.305		1.953	2.009	1.981	48.0
Q15	4	37.4	3.544		2.108	1.957	2.007	2.108	6.1
Q16	4	37.4	3.521		2.107	2.006	1.958	1.983	5.7
Q17	4	39.3	3.181		2.176	2.023	1.948	1.973	19.3
Q18	4	39.4	3.310		2.179	2.023	1.946	1.977	19.1
Q19	4	39.7	2.168			1.962	1.991	1.983	32.7
Q20	4	40.4	3.539		2.172	2.008	1.952	1.989	14.7

In the table are reported the five Cu-L distances, the dihedral angle that defines the base of the square pyramid of the N_3O_2 coordination sphere and the number of hydrogen bonds (H···O distance less than 2.0 Å). *CN* stands for coordination number

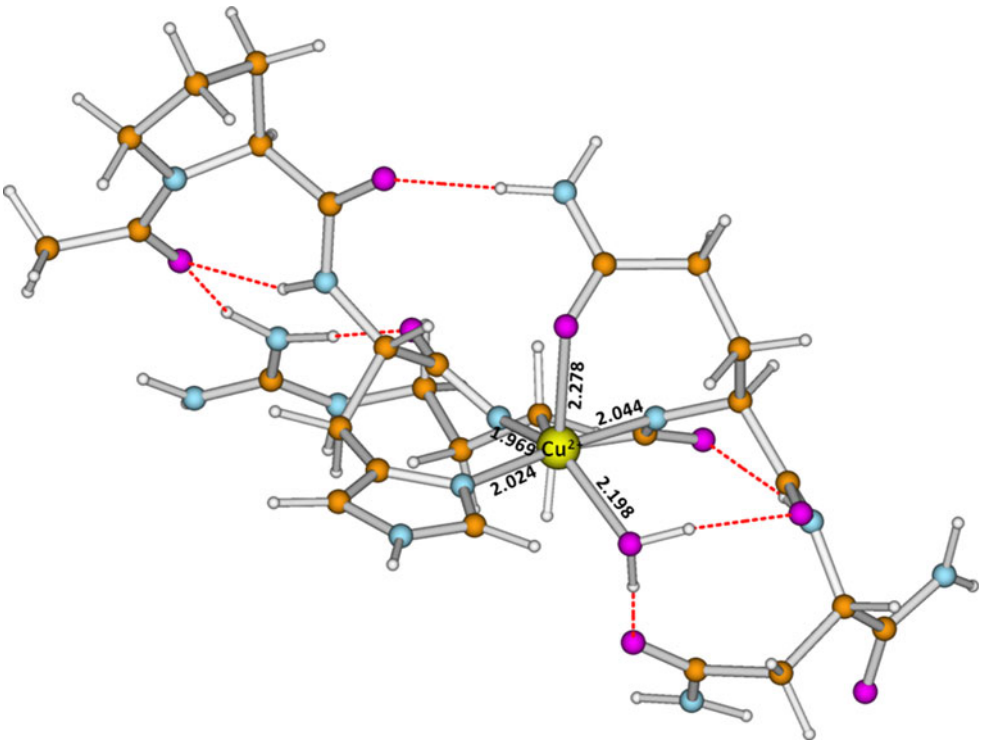

Fig. 4 Lowest-energy structure of the $[Cu(Ac\text{-}PHRQN\text{-}NH_2)(H_2O)]^{+1}$ complex (**1Q**). Distances in Å

$NH_2)(H_2O)]^{+1}$ isomer (**Q1**, see Fig. 4) features the H_2O molecule in equatorial position, whereas the carbonyl group of the glutamine side chain is coordinated to the Cu(II) atom in apical position. The high stability of **Q1** may be due to the large number of intramolecular H-bond (8). In fact, the isomer **Q2**, which is characterized by a coordination environment similar to that of **Q1**, but with a lower number of H-bond (5), is only 1.3 kcal mol^{-1} higher in energy than **Q1**. **Q3** is also close in energy to **Q1** ($\Delta E = 2.2$ kcal mol^{-1}). The latter isomer is a four-coordinated species in which the glutamine side chain has left the Cu^{2+} coordination sphere and the equatorial H_2O molecule is coordinated to the Cu atom with the shortest O-Cu distance (2.12 Å). Similarly, the isomer **Q5** is also 4-coordinated, but it is 10.3 kcal mol^{-1} higher in energy, possibly due to a smaller number of intramolecular H-bond interactions.

The lowest-energy isomer in which the carbonyl group of the glutamine side chain is coordinated to the Cu(II) atom in the equatorial position is **Q7**, which is 13.2 kcal mol^{-1} higher in energy than **Q1**. Interestingly, **Q7**, as well as all other isomers with the glutamine carbonyl group coordinated at the equatorial position (**Q15**–**Q18**), are 4-coordinated species, because the H_2O molecule leaves the Cu(II) coordination sphere.

The structures **Q8** and **Q9** are similar and are the lowest in energy among those in which the NH_2 group of glutamine is coordinated to Cu(II) atom. However, their energy is 15.2 kcal mol^{-1} higher than in **Q1**. These two isomers are also 3.0 kcal mol^{-1} less stable than **Q7** even if two more H-bond interactions are present. **Q8** and **Q9** are penta-coordinated species with the H_2O molecule weakly coordinated in apical position at about 2.5 Å from the Cu(II) atom. On the other hand, the other two isomers in which the NH_2 group of glutamine is coordinated to Cu(II) (**Q13** and **Q14**) are fully tetra-coordinated species.

3.2 EPR hyperfine coupling constants and g values of isomers of $[Cu(Ac\text{-}PHREN\text{-}NH_2)(H_2O)]$ and $[Cu(Ac\text{-}PHRQN\text{-}NH_2)(H_2O)]^{+1}$ complexes

In the previous section, it was pointed out that the energy criterion is not sufficient to confidently predict the coordination mode of Cu(II) in the $[Cu(Ac\text{-}PHREN\text{-}NH_2)(H_2O)]$ and $[Cu(Ac\text{-}PHRQN\text{-}NH_2)(H_2O)]^{+1}$ complexes, because of the different number and strength of intramolecular H-bonds in the isolated isomers, which affect their energy ranking. Therefore, in order to get a better insight into the coordination mode of these complexes, EPR ^{63}Cu hyperfine coupling constants (^{63}Cu-hcc) and g tensors of the most relevant isomers have been calculated, and compared with the experimental $A_{\parallel}$ and $g_{\parallel}$ values reported in Ref. [16]. Results are collected in Tables 4 and 5. As well known, for the Cu^{2+} ion the spin–orbit coupling (relativistic), contributions are important, due to its relatively large nuclear charge. Therefore, the Fermi contact (A_{FC}) and the principal values of the dipolar

Table 4 EPR hyperfine coupling constants (MHz) for the Cu atom in relevant isomers of the [Cu(Ac-PHREN-NH_2)(H_2O)] complex, computed using the B3LYP functional on geometries optimized at the RI-BP86/TZVP level of theory

Complex	Cu−O_{H_2O}	A^{a}_{FC}	A^{a}_{PC}	A_{iso}	$A^{a,b}_{dip}$	$A^{a,b}_{dip2}$	Total dipolar[b]	$A^{c}_{\|}$	A^{c}_{xx}	A^{c}_{yy}	δA^{d}_{dip}
1	2.645	−308	139	−170	−488; 243; 245	114; −58; −57	−373; 186; 189	−543	16	19	3
1w	2.445	−303	144	−159	−489; 244; 245	118; −61; −57	−371; 183; 188	−530	25	29	4
2	3.777	−315	132	−183	−478; 236; 241	113; −54; −60	−364, 183, 181	−547	0	−1	−1
3	3.863	−319	128	−191	−478; 238; 240	114; −55; −58	−364; 183; 182	−555	−8	−9	1
4	3.796	−310	127	−183	−478; 240; 238	112; −58; −55	−366; 182; 183	−549	−1	0	1
5	3.565	−251	140	−111	−456; 203; 252	115; −50; −65	−340; 153; 187	−451	42	76	34
6	3.374	−291	135	−155	−461; 230; 232	112, −61; −52	−349; 169; 180	−504	13	25	12
7	3.359	−320	131	−189	−468; 249; 219	113; −61; −51	−355; 188; 168	−544	−1	−21	20
8	2.488	−286	145	−141	−495; 239; 256	119; −58; −62	−376; 182; 194	−517	41	53	12
9	3.684	−321	130	−190	−479; 243; 235	114; −58; −55	−366; 185; 180	−556	−5	−10	−5
10	3.655	−244	135	−109	−432; 171; 262	109; −45; −47	−323; 126; 197	−432	16	88	72
11	2.492	−276	143	−133	−491; 241; 250	117; −57; −59	−374; 184; 191	−507	51	58	7
16	3.755	−313	134	−179	−476; 238; 239	115; −56; −60	−361; 182; 179	−540	3	0	−3
20	2.407	−230	152	−78	−468; 107; 361	111; −14; −100	−357; 93; 261	−435	17	184	167
Expt.[e]								462			

[a] A_{FC} and A_{dip} are non-relativistic Fermi contact and traceless dipolar coupling tensor, respectively. A_{PC} and A_{dip2} are the corresponding relativistic corrections

[b] The components are reported in the order A_{33}, A_{11}, A_{22}

[c] $A_{\|} = A_{iso} + A_{33}$; $A_{xx} = A_{iso} + A_{11}$; $A_{yy} = A_{iso} + A_{22}$

[d] δA_{dip} is computed as $\delta A_{dip} = A_{22} - A_{11}$ and may be considered as the deviation from the axial symmetry of the tensor

[e] Experimental values taken from Ref. [16]

Table 5 g tensors of relevant isomers of the [Cu(Ac-PHREN-NH_2)(H_2O)] complex, computed using the B3LYP functional on the geometries optimized at the RI-BP86/TZVP level of theory

	g_{iso}	g_{xx}	g_{yy}	$g_{\|}$
1	2.098	2.055	2.058	2.182
1w	2.103	2.058	2.061	2.190
2	2.092	2.048	2.053	2.175
3	2.090	2.047	2.051	2.171
4	2.088	2.046	2.050	2.170
5	2.097	2.050	2.058	2.184
6	2.095	2.049	2.055	2.180
7	2.091	2.047	2.055	2.172
8	2.106	2.059	2.060	2.192
9	2.091	2.047	2.053	2.172
10	2.093	2.044	2.058	2.177
11	2.102	2.058	2.060	2.189
16	2.093	2.049	2.054	2.177
20	2.109	2.036	2.102	2.190
Expt.[a]				2.238

[a] Experimental values taken from Ref. [16]

tensor (A_{dip}) are discussed in connection with relativistic corrections (Pseudo-contact (A_{PC}), and A_{dip2}).

All of the complexes investigated, with the exception of **5** and **10**, are characterized by a roughly planar N_3O disposition of ligands ($\delta < 20$; see Table 1). ^{63}Cu-hcc tensor components of these complexes feature an axial symmetry, as deduced from the observation that the A_{xx} ($A_{xx} \equiv A_{iso} + A_{11}$) and A_{yy} ($A_{yy} \equiv A_{iso} + A_{22}$) elements of tensor do not differ by more than 20 MHz. However, for these complexes the $A_{\|}$ ($A_{\|} \equiv A_{iso} + A_{33}$), component is significantly overestimated with respect to the experimental value (see Table 4). In this respect, it is worth noting that the $A_{\|}$ component appears to be suppressed by the axial coordination of the H_2O molecule, as deduced by the observation that in the 4-coordinated complexes (Cu−$O_{H_2O} > 3$ Å) $A_{\|} = 540$–556 MHz, whereas in **8** and **11** (Cu−$O_{H_2O} \approx 2.49$ Å) $A_{\|} = 507$–517 MHz. For the latter complexes, the $A_{\|}$ value is in better agreement with the experiment. Therefore, the comparison between experimental and computational EPR parameters might suggest a N_3O_2 (slightly distorted) square pyramidal Cu(II) coordination environment, with the H_2O molecule weakly coordinated in axial position.

Isomers **5** and **10**, which are 5.5 and 12.2 kcal mol^{-1}, respectively, higher in energy than **1**, are characterized by a significant tetrahedral distortion in the N_3O arrangement of ligands. For these two isomers, the $A_{\|}$ component is in very good agreement with the experimental value. In fact, the calculated tensor of **5** slightly deviates from the axial symmetry ($\delta A_{dip} = 34$) by a value which may not be

resolved in the experimental spectrum. A larger deviation ($\delta A_{dip} = 72$) is observed for the complex **10**. It is interesting to note that **5** and **10** are both characterized by one of the two N^{-}–Cu distances significantly shorter than in the other complexes, a feature that could also account for the depression of the $A_{\|}$ component when moving from the square planar to the distorted configuration.

The $A_{\|}$ value computed for isomer **20**, which features an equatorial H_2O molecule constrained to 2.407 Å from the Cu(II) atom, is significantly lower than the $A_{\|}$ value obtained in isomers characterized by axial coordination of the H_2O molecule, and apparently in fairly good agreement with the experimental value. However, equatorial coordination of the H_2O molecule can be ruled out since the calculated tensor components significantly deviate from ideal axial symmetry (see δA_{dip} in Table 4), a feature that is not compatible with the experimental EPR spectrum.

The computed values of g components are only slightly affected by a particular coordination mode, as reported for other copper–peptide complexes [33], and are, therefore, of little help in discriminating different isomeric forms. In general, we observe for the calculated g tensors that the trend is similar to that discussed for the ^{63}Cu-hcc parameters (see Table 5). The g tensor computed for isomer **20** exhibits a significant rhombic distortion, whereas all other isomers are characterized by an almost ideal axial symmetry of the g tensor. In addition, the $g_{\|}$ component of the penta-coordinated complexes **8** and **11** is slightly larger than that of the tetra-coordinated complexes, and in closer agreement with the experimental value.

The experimental $A_{\|}$ and $g_{\|}$ values obtained studying $[Cu(Ac\text{-}PHRQN\text{-}NH_2)(H_2O)]^{+1}$ differ from those measured for the $[Cu(Ac\text{-}PHREN\text{-}NH_2)(H_2O)]$ complex, leading to the suggestion that the carboxylate group is involved in Cu(II) coordination in the latter [16].

EPR parameters of selected $[Cu(Ac\text{-}PHRQN\text{-}NH_2)(H_2O)]^{+1}$ complexes are reported in Tables 6 and 7. As a general remark, we observe for most of the species investigated that, contrary to the experimental data, the $A_{\|}$ component of the ^{63}Cu-hcc tensor is lower than that calculated for the isomers of the $[Cu(Ac\text{-}PHREN\text{-}NH_2)(H_2O)]$ complex. Inspection of the ^{63}Cu-hcc tensor contributions reported in Table 6 shows that this behavior is mainly due to the isotropic term. The lowest-energy isomers **Q1** and **Q2** feature a similar distorted square pyramidal arrangement of ligands, with the O_{H2O} and the O_{Gln} atoms coordinated in basal and apical positions, respectively. The main difference in the coordination sphere between the two isomers lies in the O_{H2O}-Cu and O_{Gln}-Cu distances, which in **Q1** are about 0.1 and 0.04 Å shorter than in **Q2**. The $A_{\|}$ component of the ^{63}Cu-hcc tensor of **Q1** and **Q2** is smaller than the experimental value by about 90 and 40 MHz, respectively. In addition, for both isomers, the tensor is characterized by a large rhombic distortion, a feature that is not compatible with the experimental spectrum. **Q3** and **Q5** are 4-coordinated isomers in which the N_3O coordination sphere is completed by the H_2O molecule. The **Q3** complex, which is roughly planar and only 2 kcal mol^{-1} higher in energy than **Q1**, is characterized by a ^{63}Cu-hcc tensor with axial symmetry. The $A_{\|}$ component of the calculated tensor is about 60 MHz larger than the experimental value. In addition, the calculated $A_{\|}$ value is very similar to that of the square planar species in the $[Cu(Ac\text{-}PHREN\text{-}NH_2)(H_2O)]$ complex, even if the carboxylate ligand in the equatorial position is replaced by the H_2O molecule. The arrangement of ligands in **Q5**, differently from **Q3**, is characterized by a significant tetrahedral distortion. Notably, the $A_{\|}$ component of the ^{63}Cu-hcc tensor is smaller than in **Q3** and matches within 10 MHz the experimental value. In addition, the tensor deviates only slightly from the ideal axial symmetry ($\delta A_{dip} = 34$). Furthermore, this is the only isomer for which the replacement of the carboxylate ligand with the H_2O molecule increases the $A_{\|}$ value by 30 MHz, a value in very good agreement with that observed in the experiment when replacing the E residue with Q. **Q4** and **Q6** are 5-coordinated species in which the arrangement of the ligands approaches the trigonal bipyramidal symmetry. The calculated hcc tensor for these two tensors is both quantitatively and qualitatively very different from the experimental one, further indicating that the structure of the complex in solution should not deviate significantly from the square planar or square pyramidal symmetry. **Q8** is the lowest-energy isomer characterized by the equatorial coordination of four nitrogen atoms and the axial coordination of the H_2O molecule. The ^{63}Cu-hcc tensor of this isomer has axial symmetry, and the $A_{\|}$ value is about 40 MHz lower than the experimental one, indicating that this species cannot be excluded only on the basis of the computed EPR parameters. Finally, we have also calculated the ^{63}Cu-hcc tensor of **Q7**, **Q11** and **Q16** in which the carbonyl group of the glutamine side chain is coordinated to the Cu(II) atom in the equatorial position, and featuring different tetrahedral distortions ($\delta = 37.5°$, 16,3° and 5,7° for **Q7**, **Q11** and **Q16**, respectively). In **Q11**, the H_2O molecule is also weakly coordinated to the apical position. As shown in Table 6, the $A_{\|}$ component in this latter species is underestimated by more than 100 MHz with respect to the experimental value, and the tensor is characterized by a large rhombic distortion. In **Q7**, the $A_{\|}$ component is about 50 MHz smaller than in the experiment and the tensor is less affected by the rhombic distortion. In **Q16**, the $A_{\|}$ component of the ^{63}Cu-hcc tensor is in very good agreement with the experiment, and the tensor further approaches the axial

Table 6 EPR hyperfine coupling constants (MHz) for Cu atoms in relevant isomers of the $[Cu(Ac\text{-}PHRQN\text{-}NH_2)(H_2O)]^{+1}$ complex, computed using the B3LYP functional on geometries optimized at the BP86/TZVP level of theory

Complex	$Cu-O_{H_2O}$	A^{a}_{FC}	A^{a}_{PC}	A_{iso}	$A^{a,b}_{dip}$	$A^{a,b}_{dip2}$	Total dipolar[b]	$A^{c}_{\|}$	A^{c}_{xx}	A^{c}_{yy}	δA^{d}_{dip}
Q1		−206	144	−62	−452; 81; 371	111; 11; −100	−341; 70; 271	−403	8	109	101
Q2		−234	145	−89	−465; 123; 342	107; −21; −86	−358; 102; 256	−447	13	167	154
Q3		−319	133	−186	−471; 235; 236	109; −53; −56	−362; 182; 180	−548	−4	−7	−3
Q4		−120	149	29	406; 30; −436	−113; 9; 104	293; 39; −332	322	68	−304	−372
Q5	2.174	−255	126	−129	−450; 196; 254	98; −42; −57	−352; 154; 198	−481	25	69	44
Q6	2.242	−253	128	−125	−441; 80; 362	101; −11; −90	−317; 69; 272	−465	−56	147	203
Q7	3.495	−214	124	−90	−443; 178; 265	97; −37; −60	−346; 142; 205	−436	52	115	63
Q8		−234	144	−90	−461; 215; 246	111; −50; −60	−350; 165; 186	−441	76	96	−20
Q11		−165	131	−34	−456; 167; 289	110; −36; −72	−346; 131; 217	−380	97	183	96
Q16		−251	124	−127	−462; 214; 248	109; −50; −59	−353; 165; 188	−480	28	68	40
Expt.[c]								489			

[a] A_{FC} and A_{dip} are non-relativistic Fermi contact and traceless dipolar coupling tensor, respectively. A_{PC} and A_{dip2} are the corresponding relativistic corrections

[b] The components are reported in the order A_{33}, A_{11}, A_{22}

[c] $A_{\|} = A_{iso} + A_{33}$; $A_{xx} = A_{iso} + A_{11}$; $A_{yy} = A_{iso} + A_{22}$

[d] δA_{dip} is computed as $\delta A_{dip} = A_{22} - A_{11}$ and may be considered as the deviation from the axial symmetry of the tensor

[e] Experimental values taken from Ref. [16]

Table 7 g tensors of relevant isomers of the $[Cu(Ac\text{-}PHRQN\text{-}NH_2)(H_2O)]^{+1}$ complex, computed using the B3LYP functional on geometries optimized at the RI-BP86/TZVP level of theory

	g_{iso}	g_{xx}	g_{yy}	$g_{\|}$
Q1	2.106	2.023	2.100	2.184
Q2	2.102	2.036	2.088	2.181
Q3	2.091	2.048	2.055	2.171
Q4	2.102	2.030	2.094	2.182
Q5	2.085	2.041	2.056	2.159
Q6	2.090	2.026	2.083	2.161
Q7	2.084	2.037	2.058	2.157
Q8	2.098	2.051	2.063	2.179
Q11	2.091	2.039	2.065	2.169
Q16	2.084	2.043	2.050	2.160
Expt.[a]				2.240

[a] Experimental values taken from Ref. [16]

symmetry. However, **Q16** is 37.4 kcal mol^{-1} higher in energy than **Q1**, an energy difference which allow to exclude that such isomer is present in aqueous solution.

As observed for the corresponding ^{63}Cu-hcc parameters, the g tensors computed for **Q1**, **Q2**, **Q4** and **Q11** are characterized by a significant rhombic distortion, whereas in **Q3**, **Q8** and **Q11**, the tensors approach to the axial symmetry. It is worth noting that the $g_{\|}$ component of **Q16**, which features the glutamine carbonyl ligand in the equatorial position, is smaller than that of the species with the H_2O molecule in the equatorial position, a trend opposite with respect to the experimental results.

4 Conclusions

In this paper, we have reported results obtained studying Cu^{2+} coordination to the Ac-PHREN-NH_2 peptide that represents the Cu^{2+} binding portion of angiogenin, a protein playing a key role in the process of angiogenesis. Using as a reference the recent experimental results reported by La Mendola et al. [16], we have used classical MM/MD calculations followed by DFT optimizations to explore the configurational space of the [Cu(Ac-PHREN-NH_2)(H_2O)] complex.

EPR experiments suggested that Cu(II) is coordinated in a N_3O square planar environment characterized by a significant tetrahedral distortion, where the Cu(II) coordination sphere is composed by $2N^-$ of deprotonated peptide bonds, the nitrogen atom of the histidine group and the carboxylate group of the glutamic residue. An alternative N_3O_2 (less distorted) square pyramidal coordination in which the oxygen atom of a weakly coordinated water molecule occupies the apical position cannot be excluded. In addition, a detailed comparison of computed minimum energy structures and EPR parameters suggests that the binding of Cu(II) to the deprotonated amide groups of the peptide bonds takes place between the residues H-R and R-E.

We have also investigated the configuration space of the E → Q mutated system $[Cu(Ac\text{-}PHRQN\text{-}NH_2)(H_2O)]^{+1}$. In this case, computational results led to the conclusion that, similar to the [Cu(Ac-PHREN-NH_2)(H_2O)] complex, the coordination mode is described by a N_3O square planar

environment with a large tetrahedral distortion, in which the carboxylate group is replaced by a H_2O molecule. Finally, the structures that better fit the experimental EPR parameters do not correspond to the most stable isomers, further indicating that the energy ranking of isomers, derived in the absence of solvent water molecules, is not a reliable criterion in the study of speciation of metal–peptide complexes in aqueous solution.

Acknowledgments This work was supported by the PRIN Project N 200875WHMR.

References

1. Folkman J (1989) J Natl Cancer Inst 82:4
2. Bussolino F, Mantovani A, Persico G (1997) Trends Biochem Sci 22:251
3. Kishimoto K, Liu S, Tsuji T, Olson KA, Hu G (2005) Oncogene 24:445
4. Fett JW, Strydom DJ, Lobb RR, Alderman EM, Bethune JL, Riordan JF, Vallee BL (1985) Biochemistry 24:5486
5. Gao X, Xu Z (2008) Acta Biochim Biophys Sin 40:619
6. Badet J, Soncin J, Guitton JD, Lamare O, Cartwright T, Barritault D (1989) Proc Natl Acad Sci USA 86:8427
7. McAuslan BR, Reilly W (1980) Exp Cell Res 130:147
8. Hu G-F (1998) J Cell Biochem 69:326
9. Lequin O, Thuring H, Robin M, Lallemand J-Y (1997) Eur J Biochem 250:712
10. Millhauser GL (2007) Annu Rev Phys Chem 58:299
11. Solioz M, Vulpe C (1996) Trends Biochem Sci 21:237
12. Soncin F, Guitton JD, Cartwright T, Badet J (1997) Biochem Biophys Res Commun 236:604
13. Joyce BK, Cohn M (1969) J Biol Chem 244:811
14. Acharya KR, Shapiro R, Allen SC, Riordan JF, Vallee BL (1994) Proc Natl Acad Sci USA 91:2915
15. Smyth DG, Stein WH, Moore S (1963) J Biol Chem 238:227
16. La Mendola D, Magri A, Vagliasindi LI, Hansson O, Bonomo RP, Rizzarelli E (2010) Dalton Trans 39:10678
17. Halgren TA (1996) J Comput Chem 17:490
18. Halgren TA (1999) J Comput Chem 20:720
19. Becke AD (1988) Phys Rev A 38:3098
20. Perdew JP (1986) Phys Rev B 33:8822
21. Eichkorn K, Weigend F, Treutler O, Ahlrichs R (1997) Theor Chem Acc 97:119
22. Ahlrichs R, Bar M, Haser M, Horn H, Kolmel C (1989) Chem Phys Lett 62:165
23. Schafer A, Huber C, Ahlrichs R (1994) J Chem Phys 100:5829
24. Bruschi M, De Gioia L, Mitric R, Bonacic-Koutecky V, Fantucci P (2008) Phys Chem Chem Phys 10:4573
25. Schafer A, Horn H, Ahlrichs R (1992) J Chem Phys 97:2571
26. Kutzelnigg W, Fleischer U, Schindler M (1990) The IGLO-method: Ab initio calculation and interpretation of NMR chemical shifts and magnetic susceptibilities. Springer, Berlin
27. Hess BA, Marian CM, Walhgren U, Gropen O (1996) Chem Phys Lett 251:365
28. Kaupp M, Buhl M, Malkin VG (2004) Calculation of NMR and EPR parameters: theory and applications. Wiley-VCH
29. Neese F (2003) J Chem Phys 117:3939
30. Marino T, Russo N, Toscano M (2007) J Phys Chem B 111:635
31. Marino T, Russo N, Toscano M (2011) Int J Quantum Chem 111:1152
32. Pushie MJ, Rauk A (2003) J Biol Inorg Chem 8:53
33. Franzini E, De Gioia L, Fantucci P, Zampella G, Bonacic-Koutecky V (2003) Inorg Chem Commun 6:650
34. Sabolovic J, Tautermann CS, Loerting T, Liedl KR (2003) Inorg Chem 42:2268
35. Adamo C, Scuseria G, Barone V (1999) J Chem Phys 111:2889
36. Klamt A (1995) J Phys Chem A 99:2224
37. Klamt A (1996) J Phys Chem A 100:3349
38. Klamt A, Schüürmann G (1993) J Chem Soc Perkin Trans 2:799
39. Hallahan TW (1991) Proc Natl Acad Sci USA 85:5061